RESEARCH ARTICLE

ADVANCED OPTICAL MATERIALS

www.advopticalmat.de

Meta-Magnetic All-Optical Helicity Dependent Switching of Ferromagnetic Thin Films

*Muhammad Waleed Khalid, Jeongho Ha, Mohammed Salah El Hadri, Liyi Hsu, Saeed Hemayat, Yuxuan Xiao, Alexander Sergienko, Eric E. Fullerton, and Abdoulaye Ndao**

To address the ever-increasing need for higher speed and density of information storage, recent developments in ultrafast optical switching have focused on deterministic control of magnetic properties of materials using femtosecond circularly polarized optical pulses. However, a monolithic high-speed optical helicity-dependent switching at room temperature has remained elusive. In recent years, ultra-thin flat optical structures, known as metasurfaces, have been developed that offer a versatile way to manipulate electromagnetic fields using subwavelength spatial resolution. Here, a monolithic multilayer nanostructure capable of achieving optical helicity-dependent switching in arbitrary geometries using femtosecond meta-circularly polarized optical pulses is theoretically described and experimentally demonstrated at room temperature. The proposed monolithic meta-magnetic platform provides a practical route to reform the current data memory, storage, and information processing technologies in integrated opto-magnetic systems, holding great promise for cutting-edge applications in information, spintronics, sensing, and memory storage devices.

1. Introduction

Ultrafast optical manipulation of magnetization has experienced exciting developments over the last two decades, launched by the first demonstration of the ultrafast manipulation of magnetization using femtosecond (fs) laser pulses[1] and then the control of the magnetic order known as all-optical switching (AOS).[2] The deterministic magnetization switching using circularly polarized laser pulses is commonly known as all-optical helicity-dependent switching (AO-HDS), in which the helicity of the input polarization of the electromagnetic wave determines the final state of the magnetization.[3] Despite AO-HDS being successfully demonstrated in both ferri- and ferromagnetic thin films,[4–8] the mechanism of this process is still a topic of debate in the scientific community. Several models have been presented to explain AO-HDS. These include local effective fields created by the circularly polarized light via the inverse Faraday effect[9] as a source for magnetic switching. In contrast, the transfer of spin angular momentum from light to the magnetic material[10,11] and magnetic circular dichroism (MCD)[12] have also been modeled to explain AO-HDS. However, recent experiments have pointed to the fact that a contributing or even dominant mechanism of AO-HDS in ferromagnetic material is MCD. In MCD, one magnetic domain orientation favors the absorption of light with a particular helicity over the other, and temperature gradient across domain walls[13] or difference of temperature of individual grains,[14] induced by the differential absorption, switches the magnetization.

Experimental studies showed that AO-HDS of Co/Pt multilayers is a cumulative process. Indeed, initial reports showed that hundreds of ultrashort pulses[6] or several long pulses[7] are needed to achieve full AO-HDS in Co/Pt system, while a more recent study reported that the combination of one ultrashort pulse with a second longer pulse enables a more efficient and complete AO-HDS in similar Co/Pt system.[15] However, the AO-HDS symmetry-breaking mechanism remains unclear, since both the inverse Faraday effect (IFE)[16] and magnetic circular dichroism (MCD)[8] remain plausible and were proposed to explain the symmetry breaking in Co/Pt multilayers. AO-HDS

M. W. Khalid, J. Ha, M. S. E. Hadri, L. Hsu, Y. Xiao, E. E. Fullerton, A. Ndao
Department of Electrical and Computer Engineering
University of California San Diego
La Jolla, San Diego, CA 92093, USA
E-mail: a1ndao@ucsd.edu
M. W. Khalid, J. Ha, L. Hsu, S. Hemayat, A. Sergienko, A. Ndao
Department of Electrical and Computer Engineering
Photonics Center
Boston University
8 St. Mary's Street, Boston, MA 02215, USA
E. E. Fullerton
Center for Memory and Recording Research
University of California San Diego
La Jolla, San Diego, CA 92093-0401, USA

The ORCID identification number(s) for the author(s) of this article can be found under https://doi.org/10.1002/adom.202301599

DOI: 10.1002/adom.202301599

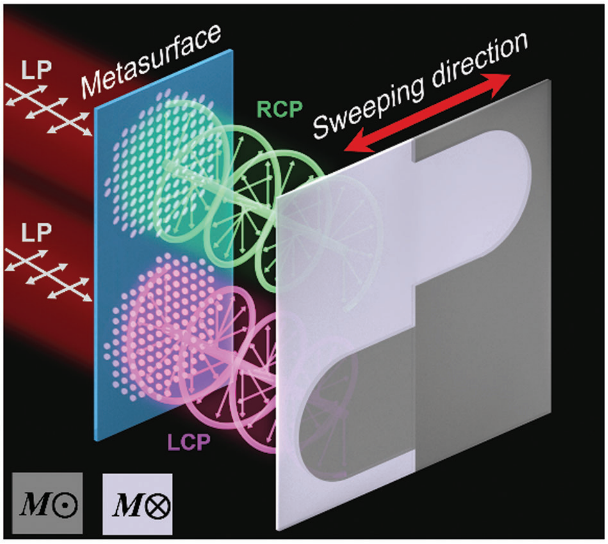

Figure 1. Schematic illustrating the meta-magnetic all-optical helicity-dependent switching (MOS). The red beams and the white arrows represent the linearly polarized incident beam. The dark and light grey domains represent out-of-plane magnetization pointing "up" ($M\odot$) and "down" ($M\otimes$), respectively. The green and pink colors represent RCP and LCP laser pulses generated by all-dielectric metasurfaces to induce optical switching. The orientation of the nanoparticles determines the direction of the circular polarization.

opens the way to manipulating magnetization at ultrafast speeds for applications in information processing and memory storage devices using optics. However, the monolithic high-density of optical helicity-dependent switching has remained inaccessible until now as its high density of elements necessitates nanostructured optical components. Metasurfaces, emerging from the broader field of metamaterials, have demonstrated many conventional and novel functionalities while being only sub-wavelength thick.[17–25] Compared with traditional optical components, a metasurface's unique planar configuration, large-scale integration, and complementary metal-oxide semiconductor processing compatibility make them well-suited to monolithic integration with optical switching structures. Here, we report and experimentally demonstrate a monolithic optical helicity-dependent magnetic switching enabled by metasurfaces. To the best of our knowledge, this is the first monolithic integration of optical helicity-dependent magnetic switching. The proposed monolithic meta-magnetic platform provides a practical route for integrating optical helicity-dependent switching with complex systems, holding great promise for cutting-edge applications in information, memory, and storage devices.

To integrate the two proliferating fields in modern science, ultrafast magnetism with metasurfaces, we combine an all-dielectric metasurface to generate circularly polarized (CP) pulses capable of AO-HDS in the [Co/Pt] ferromagnetic thin film. Our meta-magnetic platform (**Figure 1**) constitutes the metasurface quarter-wave plate generating circularly polarized light and a multilayer ferromagnetic thin film $[\mathrm{Co/Pt}]_N$, where N represents the number of bilayers in the magnetic multilayer structure. Due to the perpendicular interfacial magnetic anisotropy in the multilayer ferromagnetic thin film, the film is perpendicularly magnetized. Therefore, the image contrast results from the two possible magnetization directions. The laser pulse helicity is determined by the resonator orientation of the metasurface quarter-wave plate (m-QWP) to produce either right circular polarization (RCP) or left circular polarization (LCP). This enables us to selectively invert only one type of magnetization orientation while the other magnetization orientation remains dormant.

2. Design, Fabrication, and Characterization

2.1. Metasurface Quarter-Wave Plate (m-QWP)

To design our m-QWP, we use an array of amorphous silicon (α-Si) elliptical resonators deposited on a fused-silica substrate acting as a 2D birefringent material. **Figure 2**a presents a sketch of the α-Si metasurface unit cell and its optimized geometry parameters: $R_1 = 60$ nm, $R_2 = 110$ nm, $H = 385$ nm, and $P_x = P_y = 400$ nm. These parameters satisfy the Kerker condition[26] to maximize the measured transmission, >97% of the incident electric field. The angle of rotation of the resonator with respect to the x-axis is $\theta = \pm 45°$ depending on the desired helicity of light. $\theta = +45°$ gives RCP and the $\theta = -45°$ gives LCP at the output. Due to the anisotropy of the resonator, the metasurface only works for LP polarized along the $\vec{x}$ direction.

Figure 2b shows the broadband simulation of the all-dielectric metasurface. Numerical simulations were performed using the finite-element method (CST Microwave Studio) and the local phase method. We design our m-QWP centered at $\lambda_o = 800$ nm with 40 nm bandwidth, which converts the input LP (E_x) to output RCP (E_{LCP}) or LCP (E_{LCP}) light depending on the rotation range of the resonator w.r.t. to the input LP. The m-QWP covers the bandwidth of the incident laser pulse needed for AO-HDS centered at $\lambda_o = 800$ nm. The ratio $|E_y|/|E_x|$ is ≈ 1 and the corresponding phase difference ($\phi_y - \phi_x$) between E_y and E_x is $\approx \pi/2$ over the bandwidth of the optical pulse needed for AO-HDS. Figure 2c shows the real part of E_x and E_y inside the metasurface; as the incident field E_x passes through the resonator, half of the incident electric field couples into the E_y with a phase difference $\phi_y - \phi_x = \pi/2$. The m-QWP structure is fabricated by top-down nanomanufacturing methods and a top view of the scanning electron microscope (SEM) images for the RCP and LCP m-QWP respectively, showing a successful fabrication of the metasurface is presented in Figure 2d,e, respectively. The m-QWP in Figure 2d generates RCP and the m-QWP in Figure 2e generates LCP for a linearly polarized input light.

We used Stokes parameters (I, M, C, S) to independently characterize and evaluate the performance of the polarization state of the light transmitted out of the m-QWP.[27]

$$S = |E_{LCP}|^2 - |E_{RCP}|^2 \tag{1}$$

where $S = 1$ is for an ideal LCP and $S = -1$ is for an ideal RCP. To enable a quantitative comparison between our fabricated devices and the ideal cases. We plot them in the same figure; the comparison between the ideal, simulated, and fabricated RCP and LCP m-QWP polarization ellipses are indicated in Figure 2f,g, respectively. These polarization ellipses are extracted from the Stokes parameters averaged over the entire wavelength range of

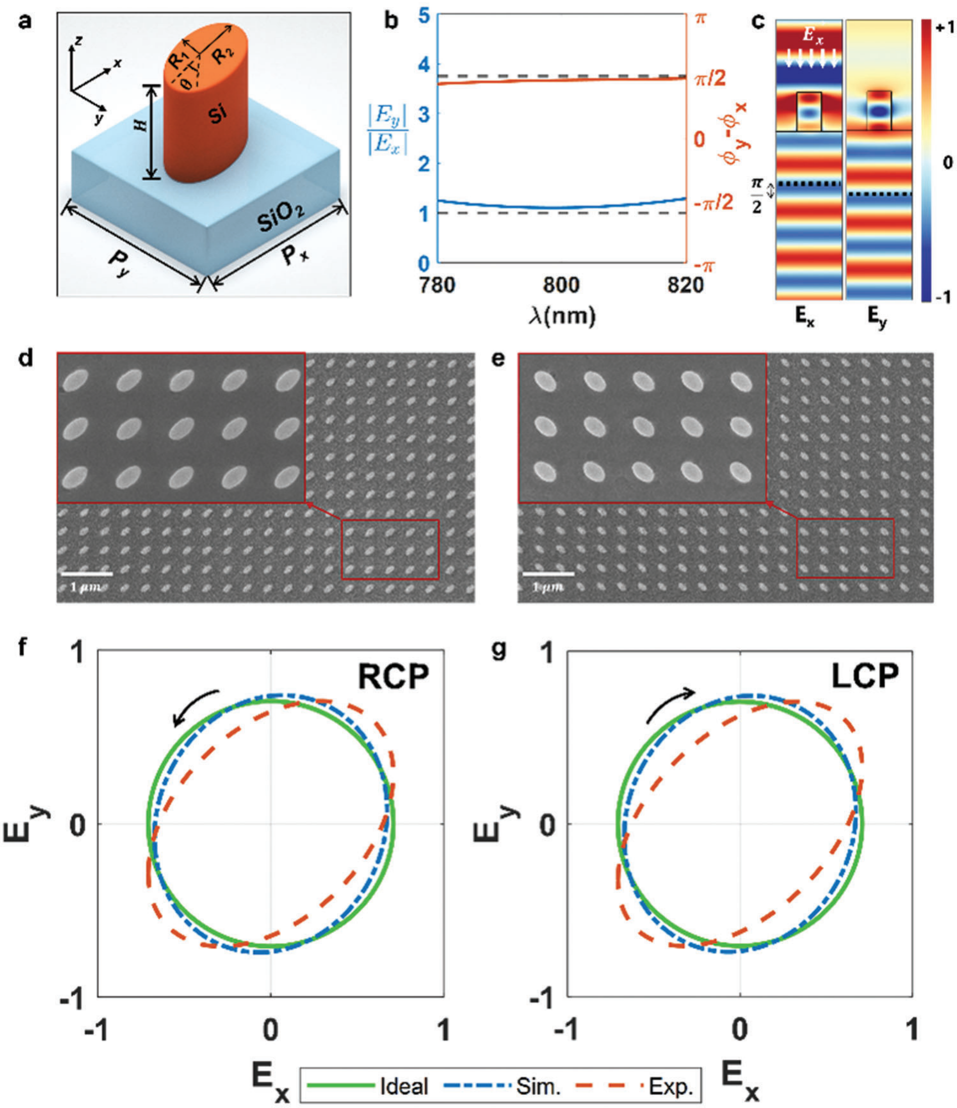

Figure 2. Meta-QWP design fabrication and measurement a) Schematic of the proposed m-QWP unit cell and its corresponding geometric parameters. b) The ratio |Ey|/|Ex| and phase difference $\phi_y - \phi_x$ between Ey and Ex over input laser pulse bandwidth. c) E_x and E_y electric field components with LP (E_x) excitation at $\lambda = 800$ nm. d,e) are top-view SEM images for RCP m-QWP ($\theta = +45°$) and LCP m-QWP ($\theta = -45°$). f,g) are polarization ellipses for ideal (green), simulated (blue), and fabricated (red) m-QWP generating RCP and LCP.

the fs laser pulse. The conversion efficiency of input linear polarization to output circular polarization, for simulated and fabricated m-QWP, is up to 91% and 97% respectively in comparison with commercial QWP, which has a conversion efficiency of 99%. The average transmission efficiency, for simulated and fabricated m-QWP, is up to 96% and 97%, respectively, in comparison with commercial QWP, which has a transmission efficiency of 99%. We successfully implemented a planar m-QWP, comparable in its AO-HDS performance to a commercial QWP shown in previous studies,[28] thus providing us with a compact alternative. These devices open a new realm of integrating metasurfaces and ultrafast magnetism in ferromagnetic materials, which we call meta-magnetic all-optical helicity-dependent switching (MOS).

The fabrication flow chart is shown in Figure S6 (Supporting Information). The m-QWPs are fabricated by a top-down etching method using a deep Silicon etching system (Oxford Plasma Lab 100 RIE/ICP) and a resist pattern mask (ma-N series). First, a thin α-Si film is deposited on a cleaned BK7 substrate using plasma enhanced chemical vapor deposition system. Then the sub-wavelength size resist patterns are formed on it using the electron beam lithography (Vistec EBPG5200) process (see Figure S2, Supporting Information, for details). Figure 2d,e are a top view of the scanning electron microscope (SEM) images for the RCP and LCP m-QWP respectively, showing a successful fabrication of the metasurface. The m-QWP in Figure 2d generates RCP and the m-QWP in Figure 2e generates LCP for a linearly polarized input light.

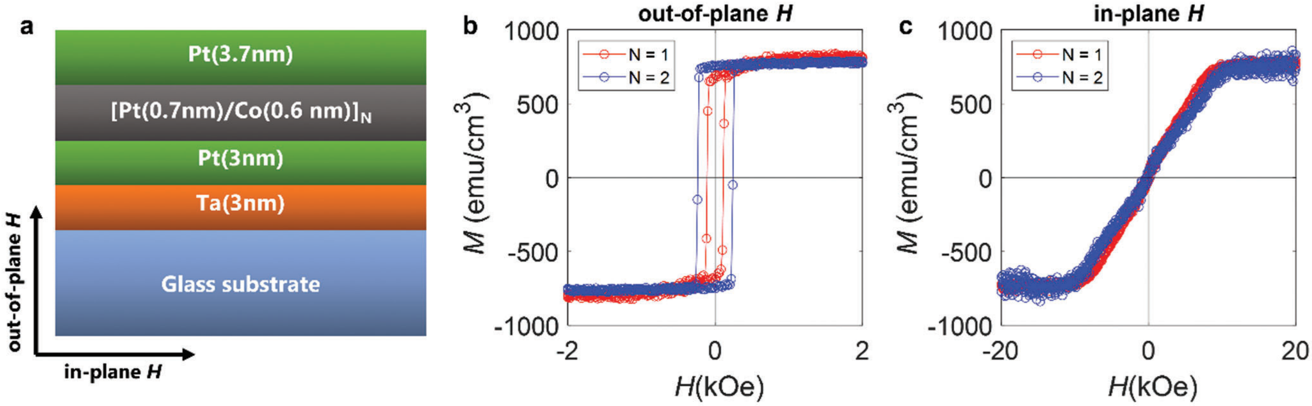

Figure 3. Room temperature VSM hysteresis loop measurement. a) Complete structure of the deposited ferromagnetic Pt/Co multilayer films, where $N = 1$ or 2. The hysteresis loops were measured for the magnetic field applied perpendicular and parallel to the plane of the samples, as shown in (b,c). Both studied ferromagnetic films exhibit strong perpendicular magnetic anisotropy and are perpendicularly magnetized.

To measure the degree of CP of the light coming out of the m-QWP, we employ an experimental Stokes polarimetry setup (see Figure S3, Supporting Information). Following this experimental scheme, the transmitted light obeys the following relationship:

$$I_T = \frac{1}{2}\{I + (M\cos 2\beta - C\sin\beta)\cos 2(\alpha - \beta) + (C\cos 2\beta - M\sin 2\beta)\cos\delta + S\sin\delta\}\sin 2(\alpha - \beta) \quad (2)$$

where δ is the retardance of the QWP, β is the angle of the QWP and α is the angle of the polarizer P with reference to input polarization. The Stokes parameters can be extracted by measuring the change in I_T as a function of the linear polarizer angle,α, or the QWP angle, β. In our measurements, we keep α fixed at 0° with respect to the input polarization and only axially translated the QWP (Thorlabs WPQSM05-808). We then use Equation (2) to calculate the Stokes parameters from I_T.

2.2. Ferromagnetic Thin Film

To demonstrate AO-HDS in ferromagnetic materials, we use perpendicularly magnetized $[Pt(0.7\ nm)/Co(0.6\ nm)]_N$ multilayers, where $N = 1$ or 2 is the number of [Pt/Co] bilayers in the thin film. The perpendicularly magnetized ferromagnetic thin films were grown on glass substrates by a DC magnetron sputtering system with a base pressure of $>3 \times 10^{-8}$ Torr. These thin films are composed of glass substrate/Ta(3 nm)/Pt(3 nm)/$[Pt(0.7\ nm)/Co(0.6\ nm)]_N$ /Pt(3.7 nm), (see **Figure 3**) where the number of repeats $N = 1$ or 2. The film deposition was performed at room temperature and in an Argon (Ar) gas atmosphere. The Ar pressure during the deposition was 2.7 mTorr for all the layers.

The ferromagnetic thin films were independently characterized using the Vibrating Sample Magnetometer (VSM) option of a VersLab system (Quantum Design, Inc., San Diego, CA). By considering the spin polarization of the Pt atoms at the interfaces by the adjacent Co layers, the saturation magnetization $M_s = 816$ emu cm^{-3} (resp. 782 emu cm^{-3}) and the uniaxial anisotropy constant $K_u = 4.38 \times 10^6$ erg cm^{-3} (resp. 3.82×10^6 erg cm^{-3}) were measured for $N = 1$ (resp. $N = 2$). The hysteresis loops are measured for a magnetic field applied perpendicular and parallel to the plane of the samples, as shown in **Figure 4**a,b, respectively. Both studied ferromagnetic films exhibit a strong perpendicular magnetic anisotropy. In our experiments, we select $N = 1$ and $N = 2$ as they satisfy the previously determined domain size criterion for AO-HDS for these films.[5]

3. Experiment and Results

Figure 3a shows a simplified version of the three monolithic configurations used in (b) and (c); LP incident on RCP m-QWP, LP incident on LCP m-QWP, and LP incident on a glass substrate (no m-QWP). Figure 3b,c shows the results of optical pulse line scans on the ferromagnetic material, with RCP and LCP generated from the m-QWP. Figure 3b shows AO-HDS for $N = 1$, and Figure 3c shows it for $N = 2$. For AO-HDS, the helicity of the fs laser pulses is controlled by the m-QWP, which transforms the LP light into the desired CP state. Using a motorized linear translation stage, the ferromagnetic sample is swept at 10 µm^{-1} s for 60 µm. The laser spot size incident on the ferromagnetic film is fixed at ≈20 µm radius, while the radius of the optically switched magnetic area is 5 µm. Therefore, to emulate a monolithic device for switching in arbitrary geometries, we make sure that the laser spot size and the corresponding fluence incident on the metasurface are the same as the laser spot size and the corresponding fluence incident on the ferromagnetic film. The laser fluence for $N = 1$ and $N = 2$ was optimized separately to achieve AO-HDS in each sample. Since the threshold power for AO-HDS increases with the repetition rate, we use fluence as the optimization parameter for the input laser pulse. Using a conventional quarter-waveplate, due to its larger size and high damage threshold, gives you the room to maneuver around the fluence needed for AO-HDS. However, in metasurfaces, we have a smaller size and lower damage threshold so we cannot maneuver too much around the fluence to observe AO-HDS. In accordance with this, the design and fabrication of this metasurface incorporate the fluence requirements needed for AO-HDS to make sure we do not damage the metasurface while operating on the fluence threshold needed for AO-HDS. During our experiments, the damage threshold of

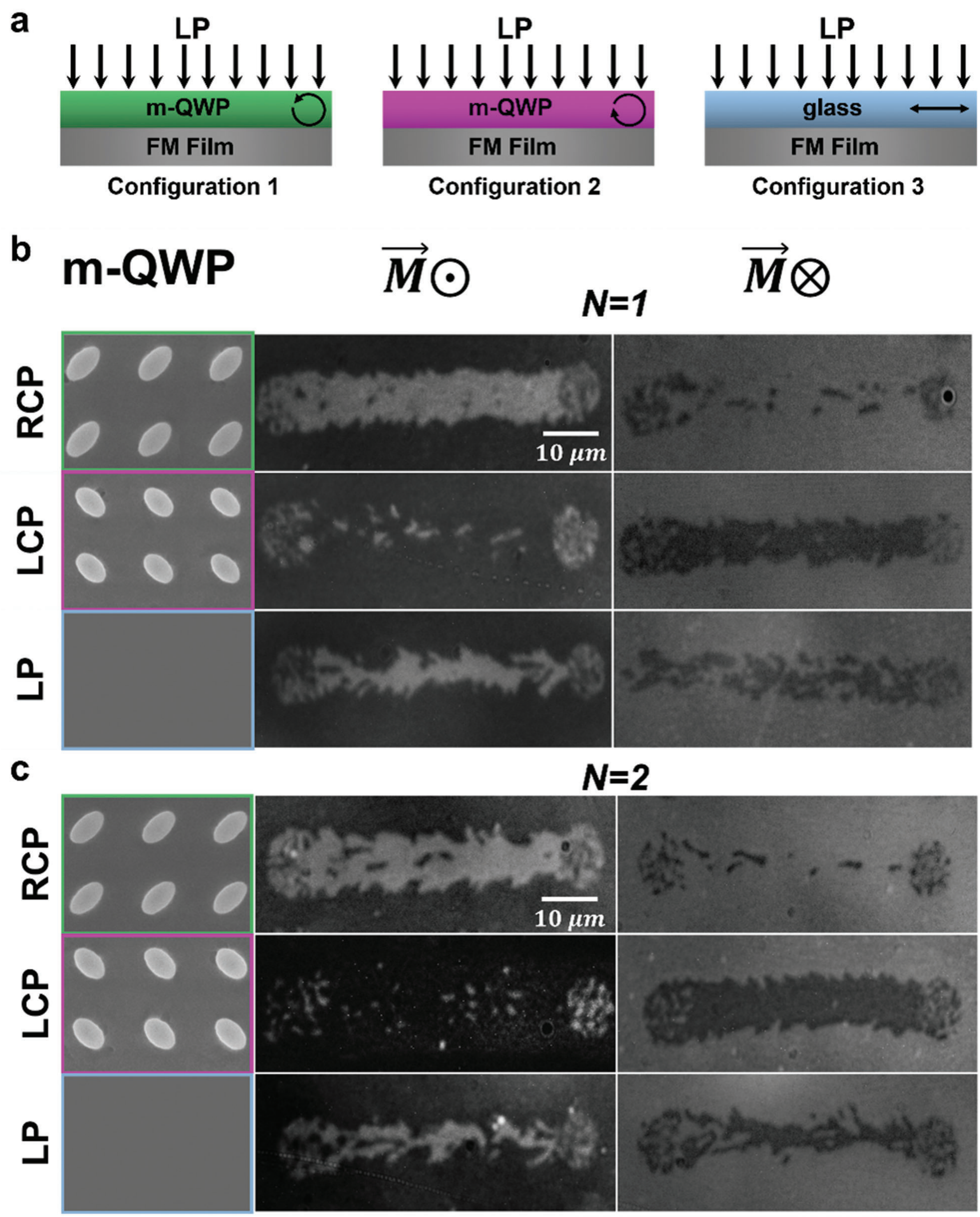

Figure 4. Magneto-optical response in zero applied magnetic fields of $[Pt/Co]_N$ multilayer samples to various laser polarizations. a) simplified versions of three configurations with incident LP on RCP m-QWP, LCP m-QWP, and glass (no m-QWP). (b,c) are results of Faraday imaging of $[Pt/Co]_N$ for different numbers of bilayers b) $N = 1$ and c) $N = 2$. For each sample, RCP, LCP, and LP optical pulses were swept over the sample from left to right. The initial magnetization saturation is shown at the top of each column in (b,c). The dark or white contrast corresponds to the reversal of the opposite of the initial magnetization. The third row in (b,c) are the results with removed metasurface and illumination of the ferromagnetic material with LP fs optical pulses.

the fabricated m-QWP was not reached when optimizing the fluence for AO-HDS, which was confirmed by imaging the metasurface after AO-HDS. To ensure this process is indeed AO-HDS, which is reversible and then repeatable, we realign the magnetization direction using a permanent magnet and then repeat the experiments on the same area of the ferromagnetic sample. To prevent temperature-dependent magnetic susceptibility changes, all measurements in the experiments were conducted at room temperature.

For a fair comparison, the fs pulses incident on the ferromagnetic material had the same fluence for all three configurations for a particular ferromagnetic multilayer repetition, N. The dark or white contrast in the figures corresponds to a reversal of the initial magnetization to the other direction. The first column in Figure 3b,c corresponds to the type of m-QWP, which will determine the incident polarization, RCP or LCP, on the ferromagnetic material and the decision on the reversal of the magnetization. The second and third columns in Figure 3b,c show the results for m-QWP induced RCP, m-QWP induced LCP, and LP incident on $[\mathrm{Pt/Co}]_N$ ferromagnetic thin films, where $N = 1$ in (a) and $N = 2$ in (b). In the second column, the initial magnetization of the sample is into the plane, $\boldsymbol{M}\odot$, while in the third column, the initial magnetization of the sample is out of the plane, $\boldsymbol{M}\otimes$. When the initial magnetization is $\boldsymbol{M}\odot$, the m-QWP RCP optical pulses reverse the magnetization, as shown by the white contrast. Meanwhile, the m-QWP-induced LCP pulses do not switch the initial magnetization, as shown by no difference in the contrast.

In circularly polarized eigen basis, LP is an equal superposition of RCP and LCP[27] and can be expressed as

$$\overrightarrow{E_{LP}} = \frac{1}{\sqrt{2}} \left(\overrightarrow{E_{RCP}} \pm i\overrightarrow{E_{LCP}} \right) \tag{3}$$

So, when LP pulses are incident on the ferromagnetic material, one can see an average of the phenomenon experienced by the ferromagnetic material concerning optical pulses of LCP and RCP. It is worth noting that when the initial magnetization is $\boldsymbol{M}\otimes$, we observe the opposite; the m-QWP-induced LCP optical pulses reverse the magnetization, as shown by the dark contrast, but the m-QWP-induced RCP pulses do not switch the initial magnetization. For $\boldsymbol{M}\otimes$ as well, the LP incident on ferromagnetic material exhibits an average effect of LCP and RCP optical pulses.

The experimental setup (Figure S8, Supporting Information) is composed of two main systems: illumination and imaging. After the initial alignment of the magnetic domains using a permanent magnet, we illuminate the sample with an optical pulse train from Ti: Sapphire laser amplifier system (Solstice from Spectra-Physics) with a central wavelength $\lambda_o = 800$ nm, 35 fs pulse duration at the source, and 1 kHz repetition rate. A spatially uniform, linearly polarized, quasi-collimated white light source (Thorlabs SLS201L), with a 650 ± 40 nm bandpass filter, is incident on the sample and is collected by a 40× apochromatic objective lens for observing AO-HDS in the ferromagnetic film. LED's initial polarization rotates due to the Faraday effect depending on the sample's magnetization ($\boldsymbol{M}\otimes$ or $\boldsymbol{M}\odot$). The clockwise or anti-clockwise direction of light polarization rotation depends on the orientation of the magnetization inside the sample and on the analyzer angle. A monochromatic CMOS camera enables us to capture the impact of these different magnetization orientations on the sample. A 50/50 beam-splitter is used to overlap the imaging source and the laser beam, allowing for direct imaging of magnetization after the laser excitation. In our experience, we have observed that magnetization has maintained the switched up/down state for at least 6 months. This number could also be longer if the environmental conditions don't perturb the systems. We have performed more than 1500 cycles on a single sample, and there has been no degradation or change in the process of AO-HDS.

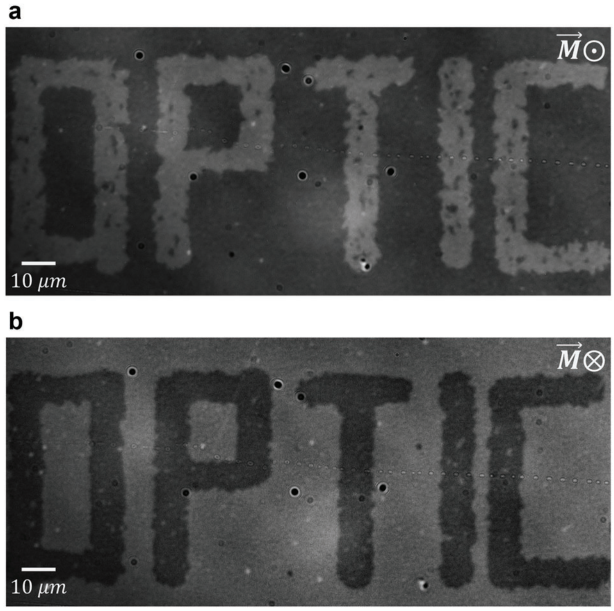

Figure 5. Arbitrary geometry meta-magnetic all-optical helicity dependent switching OPTIC is written using m-QWP on $N = 1$ ferromagnetic material. a) The initial magnetization is M⊙ and the incident fs laser pulses on the sample are RCP b) The initial magnetization is M⊗ and the incident fs laser pulses on the sample are LCP.

To further demonstrate the m-QWP functionality, we use the same custom setup (see Figure S8, Supporting Information) to show that the m-QWP can switch the magnetization in arbitrary geometries, as shown in **Figure 5**. To do so, we use a 2D motorized translation stage and an external optical shutter, to block the optical pulses when transitioning from one alphabet to the other, all controlled using MATLAB. The line scans first optimized the laser fluence and translation stage speed as in Figure 3. The optical shutter and the translation stages were then appropriately automated to block/unblock the optical pulse and translate it into the desired geometry. The entire process of writing the word "OPTIC" takes about 5 min, and the laser stays on the m-QWP without damaging it. The measured damage threshold of the metasurface is ≈16 mJ cm^{-2}. The present result supports our fabricated m-QWP's ability to withstand long exposures to high-power lasers. Since AO-HDS relies on the fluence of the fs laser pulses, the m-QWP must tolerate the fluence needed for AO-HDS any damage. Our work thus brings metasurfaces to a new platform not demonstrated previously.

4. Conclusion

We propose and experimentally demonstrate a monolithic multilayer nanostructure capable of achieving high-speed optical helicity-dependent switching using femtosecond meta-circularly polarized optical pulses at room temperature. The interaction between heat effects and all-optical switching (AOS) offers substantial research opportunities from a broader perspective. Future research could go into greater depth to comprehend the long-term heat effects on AOS, providing crucial information for enhancing magnetic storage and computing systems. Our proposed monolithic meta-magnetic platform provides a practical route to reform the current data storage and information processing technologies in complex systems, holding great promise for cutting-edge applications in information, spintronics, quantum computing, sensing, and memory storage devices.

Supporting Information

Supporting Information is available from the Wiley Online Library or from the author.

Acknowledgements

M.W.K., J.H., and M.S.E.H. contributed equally to this work. This work was supported by the 2023 Beckman Young Investigator Award from the Arnold and Mabel Beckman Foundation, the Air Force Office of Scientific Research MURI award number FA9550-22-1-0312, the PAIR-UP program sponsored by ASCB and funded in part by The Gordon Moore Foundation with additional support from the Burroughs Wellcome Funds, 2022 Scialog: Advancing BioImaging, the Kavli Innovation Grant, and the National Science Foundation, Division of Materials Research (Award #: 2105400).

Conflict of Interest

The authors declare no conflict of interest.

Data Availability Statement

The data that support the findings of this study are available from the corresponding author upon reasonable request.

Keywords

ferromagnetic materials, meta-magnetic, metasurfaces

Received: July 11, 2023
Revised: August 9, 2023
Published online:

[1] E. Beaurepaire, J.-C. Merle, A. Daunois, J.-Y. Bigot, *Phys. Rev. Lett.* **1996**, *76*, 4250.
[2] F. Hellman, A. Hoffmann, Y. Tserkovnyak, G. S. D. Beach, E. E. Fullerton, C. Leighton, A. H. MacDonald, D. C. Ralph, D. A. Arena, H. A. Dürr, P. Fischer, J. Grollier, J. P. Heremans, T. Jungwirth, A. V. Kimel, B. Koopmans, I. N. Krivorotov, S. J. May, A. K. Petford-Long, J. M. Rondinelli, N. Samarth, I. K. Schuller, A. N. Slavin, M. D. Stiles, O. Tchernyshyov, A. Thiaville, B. L. Zink, *Rev. Mod. Phys.* **2017**, *89*, 025006.
[3] A. Kirilyuk, A. V. Kimel, T. Rasing, *Rev. Mod. Phys.* **2010**, *82*, 2731.
[4] C.-H. Lambert, S. Mangin, B. S. D. Ch. S. Varaprasad, Y. K. Takahashi, M. Hehn, M. Cinchetti, G. Malinowski, K. Hono, Y. Fainman, M. Aeschlimann, E. E. Fullerton, *Science* **2014**, *345*, 1337.
[5] M. S. El Hadri, M. Hehn, P. Pirro, C.-H. Lambert, G. Malinowski, E. E. Fullerton, S. Mangin, *Phys. Rev. B* **2016**, *94*, 064419.
[6] M. S. El Hadri, P. Pirro, C.-H. Lambert, S. Petit-Watelot, Y. Quessab, M. Hehn, F. Montaigne, G. Malinowski, S. Mangin, *Phys. Rev. B* **2016**, *94*, 064412.
[7] G. Kichin, M. Hehn, J. Gorchon, G. Malinowski, J. Hohlfeld, S. Mangin, *Phys. Rev. Appl.* **2019**, *12*, 024019.
[8] Y. Quessab, R. Medapalli, M. S. El Hadri, M. Hehn, G. Malinowski, E. E. Fullerton, S. Mangin, *Phys. Rev. B* **2018**, *97*, 054419.
[9] K. Vahaplar, A. M. Kalashnikova, A. V. Kimel, S. Gerlach, D. Hinzke, U. Nowak, R. Chantrell, A. Tsukamoto, A. Itoh, A. Kirilyuk, T.h. Rasing, *Phys. Rev. B* **2012**, *85*, 104402.
[10] C. D. Stanciu, A. V. Kimel, F. Hansteen, A. Tsukamoto, A. Itoh, A. Kirilyuk, T.h. Rasing, *Phys. Rev. B* **2006**, *73*, 220402.
[11] G. Malinowski, F. Dalla Longa, J. H. H. Rietjens, P. V. Paluskar, R. Huijink, H. J. M. Swagten, B. Koopmans, *Nat. Phys.* **2008**, *4*, 855.
[12] Y. Quessab, M. Deb, J. Gorchon, M. Hehn, G. Malinowski, S. Mangin, *Phys. Rev. B* **2019**, *100*, 024425.
[13] R. Medapalli, D. Afanasiev, D. K. Kim, Y. Quessab, S. Manna, S. A. Montoya, A. Kirilyuk, T.h. Rasing, A. V. Kimel, E. E. Fullerton, *Phys. Rev. B* **2017**, *96*, 224421.
[14] Y. K. Takahashi, R. Medapalli, S. Kasai, J. Wang, K. Ishioka, S. H. Wee, O. Hellwig, K. Hono, E. E. Fullerton, *Phys. Rev. Appl.* **2016**, *6*, 054004.
[15] K. T. Yamada, A. V. Kimel, K. H. Prabhakara, S. Ruta, T. Li, F. Ando, S. Semin, T. Ono, A. Kirilyuk, T. Rasing, *Front. Nanotechnol.* **2022**, *4*, 765848.
[16] T. D. Cornelissen, R. Córdoba, B. Koopmans, *Appl. Phys. Lett.* **2016**, *108*, 142405.
[17] N. Yu, P. Genevet, M. A. Kats, F. Aieta, J.-P. Tetienne, F. Capasso, Z. Gaburro, *Science* **2011**, *334*, 333.
[18] N. Yu, F. Capasso, *Nat. Mater.* **2014**, *13*, 139.
[19] A. Arbabi, Y. Horie, M. Bagheri, A. Faraon, *Nat. Nanotechnol.* **2015**, *10*, 937.
[20] W. T. Chen, A. Y. Zhu, M. Khorasaninejad, Z. Shi, V. Sanjeev, F. Capasso, *Nano Lett.* **2017**, *17*, 3188.
[21] A. Ndao, L. Hsu, J. Ha, J.-H. Park, C. Chang-Hasnain, B. Kanté, *Nat. Commun.* **2020**, *11*, 3205.
[22] N. Yu, F. Aieta, P. Genevet, M. A. Kats, Z. Gaburro, F. Capasso, *Nano Lett.* **2012**, *12*, 6328.
[23] A. M. Shaltout, V. M. Shalaev, M. L. Brongersma, *Science* **2019**, *364*, eaat3100.
[24] J. M. Abendroth, M. L. Solomon, D. R. Barton, M. S. El Hadri, E. E. Fullerton, J. A. Dionne, *Adv. Opt. Mater.* **2020**, *8*, 2001420.
[25] S. Divitt, W. Zhu, C. Zhang, H. J. Lezec, A. Agrawal, *Science* **2019**, *364*, 890.
[26] R. Alaee, R. Filter, D. Lehr, F. Lederer, C. Rockstuhl, *Opt. Lett.* **2015**, *40*, 2645.
[27] E. Collett, *Field Guide to Polarization*, SPIE, Bellingham, WA **2005**.
[28] A. V. Kimel, M. Li, *Nat. Rev. Mater.* **2019**, *4*, 189.